In Vivo Multi-Day Calcium Imaging of CA1 Hippocampus in Freely Moving Rats Reveals a High Preponderance of Place Cells and No Detectable Photobleaching

Hannah S Wirtshafter[1*], John F Disterhoft[1]

*Lead contact: hsw@northwestern.edu (HSW)

1. Department of Neuroscience, Northwestern University Feinberg School of Medicine, Chicago, IL, USA.

Abstract

Calcium imaging using GCaMP calcium indicators and miniature microscopes has been used to image cellular populations during long timescales and in different task phases, as well as to determine neuronal circuit topology and organization. Because the hippocampus (HPC) is essential for many tasks of memory, spatial navigation, and learning, calcium imaging of large populations of HPC neurons can provide new insight on cell changes and organization over time during these tasks. To our knowledge, all reported HPC *in vivo* calcium imaging experiments have been done in mouse. However, rats have many behavioral and physiological experimental advantages over mice, and, due to their larger size, rats are able to support larger implants, thereby enabling the recording of a greater number of cells. In this paper, we present the first *in vivo* calcium imaging from CA1 hippocampus in freely moving rats. Using GCaMP7c and the UCLA Miniscope, we demonstrate that hundreds of cells (mean 240+-90 cells per session, maximum 428 cells) can reliably be visualized and held across weeks, and that calcium events in these cells are correlated with periods of movement. We additionally show proof of method by showing that an extremely high percent of place cells (82.3%+-8.1%, far surpassing the percent seen during mouse calcium imaging) can be recorded on a navigational task, and that these place cells enable accurately decoding of animal position. Finally, we show that calcium imaging in rats is not prone to photobleaching during hour-long recordings and that cells can be reliably recorded for an hour or more per session. A detailed protocol for this technique, including notes on the numerous parameter changes needed to use Ca2+ imaging in rats, is included in the Materials and Methods section, and implications of these advancements are discussed.

Introduction

The explosion in the use of *in vivo* calcium imaging has allowed the visualization of hundreds of identified neurons over long time periods [1-8]. Calcium (Ca2+) imaging using GCaMP calcium indicators and miniature microscopes has been used to image cellular populations during long timescales [9-15] and in different task phases [16-18], as well as to determine neuronal circuit topogrophy and organization [19-22].

The hippocampus (HPC) has been studied with cellular resolution using *in vivo* electrophysiology, but this technique does not allow the same cells to be definitively followed over days, nor does it allow the visualization of cellular organization within the structure [23-27]. *In vivo* calcium imaging is particularly well suited for imaging the rodent HPC, as the orientation of the horizontal cell layer permits imaging of large numers of neurons with insertion of a 1mm diameter or smaller lens [12, 13, 22, 28]. Because the hippocampus is essential for many tasks involving memory [15, 29-37], spatial navigation [38-43], and learning [44-47], Ca2+ imaging of large populations of HPC neurons can shed new insight on cell changes and organization over time during these tasks.

To our knowledge, all reports of hippocampal *in vivo* calcium imaging have been done in mouse (although calcium imaging has been used to visualize other structures in rat [48-51]). Using calcium imaging in rat hippocampus requires optimizing a number of methodological parameters, including aspiration and lens implantation techniques, to account for the increased thickness of the rat alveus compared to mouse which makes focusing on the CA1 cell layer difficult [52-54]. However, rats have many basic experimental advantages over mice: First, rats are able to learn and perform more complex tasks than mice, and employ more advanced strategies, and are thus suited for a wider variety of behavioral experiments [55-60]. Second, compared to mouse physiology, rat physiology for a number of conditions and disorders (including addiction, aging, and schizophrenia, among others) more closely mirrors human physiology [61-64]. Third, rats are less stressed by handling than mice, thus introducing less variability in experimental procedures [65].

Rats are also an advantageous organism to use for calcium imaging: Due to their larger size, rats are able to support larger implants, including a wider diameter imaging lens and a larger camera, thereby enabling the recording of a greater number of cells [2, 66, 67]. Additionally, rat hippocampal neurons are less excitable than those in mice [54, 59], and rats are less prone to post-operative seizures than mice [68-70]. Rats may therefore, compared to mice, be at a decreased risk of the seizures (and potentially to cell death) seen in mice after prolonged GCaMP expression [5, 6, 71-73].

Although *in vivo* Ca2+ imaging would appear to hold substantial promise for the study of hippocampus in freely moving rats, there is currently no direct evidence that it will work in this system. To our knowledge, there are no studies employing Ca2+ imaging in rats, and the technique appears to have obtained a reputation for being difficult to use successfully to image rat CA1. In this paper, we present the first (to our knowledge) *in vivo* Ca2+ recording from CA1 hippocampus in freely moving rats. We demonstrate that hundreds of cells are reliably visualized and held across weeks using this technique, and that there is little to no loss of fluorescence even in long (30-60m) recording sessions. We additionally show proof of method by showing that a uniquely high percentage (>80%) of place cells were recorded on a navigational task involving retrieving food reward on a linear track. A detailed protocol for this technique, including notes on the numerous parameter changes needed to use Ca2+ in rats, is included in the Materials and Methods section, and implications of these advancements are discussed.

Results

To initiate Ca2+ imaging, we injected AAV9-Syn-GCaMP7c below the CA1 cell layer in five male Fischer 344 x Brown Norway rats (Figure 1a, see Materials and Methods) [74]. After injection, in the same surgery, cortex and corpus collosum were aspirated through a craniotomy until the alveus was clearly visible (Figure 1b, see Materials and Methods). A 2mm diameter GRIN lens was inserted into the craniotomy and cemented in place. Three animals were checked for GCaMP expression four weeks

after surgery, and all three animals showed expression and were subsequently affixed with a base plate to secure the position of the miniscope. The other two animals were checked six weeks after surgery and showed expression and were base plated. After the completion of the experiment, animals were sacrificed and expression of GCaMP in CA1 pyramidal cells was verified with microscopy (Figure 1c).

Animals were then food deprived to 85% body weight and trained on a 2.64m linear track (Figure S1a). Animals were rewarded with grain pellets on alternating sides of the linear track and quickly learned to run back and forth on the track (Figure S1b). A visit to one reward well signified a trial. Animals were run for a minimum of 30 minutes or 50 trials, whichever came later, with total track time not to exceed one hour per session. Cells were recorded for 7 days for one animal, 11 days for one animal, and 16 days for two animals (n=4 rats, one of the five animals was eliminated when the implant was lost).

Six sessions were analyzed from each animal, with first and last recorded sessions automatically included. These sessions were analyzed for cellular activity using the CNMF-E method implemented by the CIATAH software package [75-77] (See Materials and Methods). A total of 5761 neurons were recorded over the 24 sessions, with a maximum of 428 cells from a single session (mean of 239.6+-90.0 cells) (Figure 2a-d). Calcium activity appeared to be heavily modulated by the animal's activity, with periods of higher activity when the animal was running rather than stationary on the track (Figure 2c). The number of cells recorded from each animal across sessions was relatively constant (Figure 2d).

We then determined if there were place cells on any of the trials. A cell was considered to be a place cell if it met two criteria: First, the cell must have a mean firing rate greater than 0.01Hz. Second, the mutual information (MI) computed in either direction of travel must be greater than 95% of MI scores computed 500 times from shuffled cells [78]. Based on these criteria, all trials contained place cells (Figure 3a, Figure S2). An average of 82.3%+-8.1% of cells with firing rates >0.01Hz were place cells (Figure 3b-c).

140 We then aimed to determine whether place cell firing was sufficient to decode the
141 position of the animal. We split the track in 10cm segments and used Bayesian
142 decoding to determine the position of the animal in non-overlapping 0.5 second
143 increments [79]. We found that the best positional decoding was accurate to a median
144 error of 4.3cm (1.6% of the 2.64m track). Across all animals, accuracy ranged from a
145 median of 4.3cm to 13.6cm (decoding errors were below 10cm in 23 sessions and
146 above 10cm in one session) with a median error of 5.9cm (Figure 4a). To confirm that
147 decoding accuracy was better than chance we shuffled firing rate per position bins and,
148 using the shuffled data, decoded position. Median error for shuffled data ranged from
149 59.1cm to 77.6cm, which was significantly worse than non-shuffled data (Kruskal-Wallis
150 test, $x^2(47)= 35.3$, $p=2.9*10^{-9}$) (Figure 4b).
151 We then aimed to determine if the same cells could be held over the duration of
152 our recordings (six recording sessions, spanning 7, 11, or 16 days). 40% of the cells
153 imaged on day one of the 7 day session were also present on day seven. Of the rat run
154 for 11 days, 31% of the cells present on day one were also present on day eleven. For
155 the two rats run 16 days, 28% and 50% of cells, respectively, that were present on day
156 one were also present on day sixteen. Across all four animals, cells that were imaged
157 on day one of recording had, on average, a 72+-6% chance of being imaged on at least
158 one subsequent day of recording (Figure 5a). (Of note, recordings each day were made
159 to optimize total cell number in each day as proof of method, rather than to maintain the
160 same landmarks or focal planes.)
161 Finally, our recording times lasted up to an hour per day, but we observed
162 obvious no photobleaching within our sessions. We thus aimed to quantify if GCaMP
163 photobleaching occurred within each session. To determine this, we compared the
164 mean fluorescence of each cell for five minutes at the start of each session to the mean
165 fluorescence of each cell for five minutes at the end of the session [80]. We found there
166 was no consistent loss of fluorescence (mean change = .008, median change = -
167 $2.01*10^{-4}$) (Figure 5b). In 22 out of the 24 sessions, the end mean fluorescence of each
168 cell was not less than the starting mean fluorescence (one-tailed paired t-test, $p>0.05$),
169 and for 6 of these sessions, the end mean fluorescence was actually greater than the

starting fluorescence (one-tailed paired t-test, $p<0.05$). Two sessions (8% of sessions) showed a decrease in fluorescence (one-tailed paired t-test, $t(368)=2.47$, $p<0.01$, and $t(231)=1.98$, $p<0.05$). We questioned whether the lack of decrease in fluorescence might have been due to an increase in calcium events in the latter part of the session, so we compared the number of events for each cell in the early five-minute period with the late five-minute period. In every session, there were not significantly more calcium events in the latter five-minute period than in the former (one-tailed paired t-test, $p>0.05$). To additionally control for the number of calcium events, we normalized the fluorescence in each five-minute period by the number of events in the period, and then found the change in fluorescence from beginning to end of session (mean change = $-1.77*10^{-4}$, median change = $-5.7*10^{-8}$)(Figure 5c). Even after normalization, still only two sessions (although a different two) showed a decrease in fluorescence from the start period to the end period (one-tailed paired t-test, $t(226)=1.7$, $p=0.04$, and $t(349)=2.1$, $p=0.02$), while three sessions showed an increase (one-tailed paired t-test, $t(123)=-1.9$; $p=0.03$, $t(173)=-3.0$, $p<0.005$; $t(166)=-4.0$, $p<0.00005$). There was therefore no consistent loss of fluorescence within each session.

Discussion

In this manuscript, we have demonstrated calcium imaging recordings can be performed in the CA1 region of the hippocampus in freely moving rats. These recordings can capture hundreds of cells in a single recording session, including a high number and percentage of place cells sufficient to decode the animal's position to within centimeters of accuracy. We additionally showed that recordings are stable across time, and that there is no evidence of significant photobleaching during recording. Calcium imaging in rat will allow for more behaviorally complex and translational experiments than have been done in mouse.

Significantly, we found a higher percentage of place cells in our calcium imaging experiments in rats than those reported in mouse CA1 calcium imaging experiments, even after the mice experiments were corrected for cells with low spiking rates. (The

200 studies with mice reported 20-30% of imaged CA1 cells were place cells, which is also
201 substantially below most electrophysiology experiments [14, 81]). Previous work has
202 reported that mouse place cells are less spatially tuned, contain less spatial information,
203 and have less stable place fields than in rat [59, 82], so some of the difference in place
204 cell percent may be due to species differences in spatial representations. However,
205 there are also likely physiological differences between rats and mice that affect the type
206 of activity captured in calcium imaging recordings. CA1 cells in mice are more excitable
207 than those in rat [54, 59], and prolonged GCaMP expression in mice has been shown to
208 lead to cell hyperexcitability, seizures, and even cell death [5, 6, 71-73]. The higher
209 baseline excitably of mouse cells, combined with a further increase in cellular excitability
210 after GCaMP expression may result in a lower threshold for cell firing and less defined
211 place fields, less stable fields, and, therefore, a seemingly lower number of place cells
212 compared to electrophysiology recordings [59]. Because rats have a lower baseline
213 excitability, they may be less prone to these GCaMP effects, although further slice
214 electrophysiology work will need to be done to directly compare the effect of GCaMP on
215 mouse and rat neurons.
216 The percentage of hippocampal CA1 cells found to be place cells using calcium
217 recordings (82.3%) was also slightly above findings from electrophysiological data,
218 which report that 35-75% of CA1 pyramidal cells recorded on a navigational task are
219 place cells (the number varies widely depending on task parameters) [83-85]. There are
220 multiple possible reasons related to recording technology as to why our calcium imaging
221 experiments detected a higher percentage of place cells than traditional
222 electrophysiology experiments: First, the GCaMP we used (AAV-syn-jGCaMP7c)
223 appeared to be preferentially expressed in pyramidal neurons (Figure 1c), which has
224 previously been reported at specific titers [74]. We are therefore preferentially imaging
225 cells that are expected to have place fields; while place information can be extracted
226 from CA1 inhibitory interneurons, they do not have place fields [86]. (Although
227 interneurons are typically removed from place field electrophysiological place cell
228 analysis, this can be difficult to do in practice.) Second, in electrophysiology
229 experiments with moveable electrodes (such as tetrodes), electrodes are typically

230 positioned while rats are inside a “sleep box” or other non-training apparatus until cells
231 are detected. The animal is then placed on a track for experimentation. This practice
232 optimizes cell detection for place cells that are active in the “sleep box” rather than on
233 the track. Because calcium imaging uses a fixed lens location and images a large
234 number of cells at once, recording is not optimized for a particular environment. This
235 may result in the recording of a higher percentage of active place cells on the recording
236 apparatus. Finally, compared to electrophysiology, calcium imaging provides additional
237 characteristics (cell shape, size, and brightness) by which to separate adjacent or
238 nearby cells. Because conflation of multiple cells may disguise place fields and disrupt
239 place field measurements (such as mutual information or bits per spike), the additional
240 resolution afforded by calcium imaging may allow for more accurate place cell
241 differentiation and identification.

242 In addition to potentially allowing the recording of a higher number of place cells,
243 the lower excitability of rat CA1 neurons, compared to mouse, also has other
244 advantages. We saw no behavioral evidence of post-operative seizures in any of our
245 implanted animals, and no behavioral or imaging evidence of seizures several months
246 post viral injection and lens implementation. This is in contrast to calcium imaging
247 experiments in mice, which frequently report that animals have to be removed from
248 behavior or analysis due to the development of seizure activity [71, 87].

249 Rats’ larger weight and body size also allows the implantation of a larger lens
250 (we used a 2mm diameter lens, as opposed to the 0.5mm or 1.0mm lenses typically
251 used in mouse CA1 imaging, and believe larger lenses could also be used), which in
252 turn allows for the imaging of larger areas and more cells. It also appears that, unlike in
253 mouse calcium imaging experiment, where cells are often not imaged for longer than
254 10min periods to avoid photobleaching [8, 13, 78], cells in rat hippoocampus can be
255 reliably recorded for an hour or more without any adverse effects on brightness (Figure
256 5b-c). Although the reason for this remains unclear, there is evidence that larger cells
257 may show less photobleaching [88]. The larger pyramidal neurons in the rat than mouse
258 [54] may therefore contribute to the reduction of photobleaching. Rats’ lower baseline
259 excitability may also cause less baseline calcium expression, resulting in fewer chances

260 for photobleaching. Regardless, the ability to do long (60+ min) recording experiments
261 provide another compelling reason to use rats in calcium imaging experiments.
262 During our recording sessions, we saw clear evidence that calcium events were
263 strongly correlated with periods of movement (Figure 2c). This result is similar to
264 calcium imaging experiments done in mice by Zhou et al., in which more calcium events
265 were seen during movement in an environment where food reward could be obtained
266 than during quiet wakefulness in a neutral box [8]. In our experiment, periods of quiet
267 wake were in the same environment (the track) as periods of movement, which shows
268 that changes in calcium event frequency are related to movement and not to contextual
269 associations. Zhou et al. posit that the high amount of calcium activity state-dependent
270 during movement, but not during sharp wave ripples in mouse, implicate calcium events
271 in theta dependent processes, such as memory encoding and planning [89-95]. Further
272 work will be needed to determine if, in rat, frequent calcium events are also unique to
273 movement, as opposed to sharp wave ripples.
274 As previously mentioned, similarities between rat and human physiology, as well
275 as the increased capacity for complex tasks of learning and memory [55-60], position
276 rats as a well-suited model organism for studying hippocampal function, with several
277 advantages over the mouse. Rats are advantageous over mice in that, for many
278 diseases and disorders, including those with substantial hippocampal involvement, their
279 physiology and behavior more closely mirrors that of humans [63]. For instance, 5-HT
280 serotonin receptors, which are prominent in the hippocampus and are implicated in a
281 variety of disorders (including mood and anxiety disorders, psychiatric disorders such as
282 schizophrenia, addiction and ADHD), are distributed in rats, but not in mice, in a similar
283 pattern as seen in humans [63, 96]. Hippocampal neurogenesis, which is believed to
284 play an important role in learning, memory, and the treatment of depression, is believed
285 to follow a similar pattern in rats and humans, and is less pronounced in mice [97]. In
286 addition, both pharmacologic and behavioral responses to addiction are more similar
287 between rats and humans than mice and humans [63, 98, 99].
288 Having the ability to do calcium imaging in rat CA1 will allow increased research
289 into these disorders, as well as basic research in learning and memory. Because rats

are substantially larger than mice, they can support larger lens implants and cameras, which may lead to the ability to record from thousands of hippocampal cells in a single session during complex tasks. The ability to record a large number of cells across days will allow research into cell firing changes in the hippocampus, which will provide insight into more advanced learning and disease mechanisms that are difficult to understand when only investigating mice. Additionally, the uniquely high percentage of recorded place cells (>80% of recorded cells) makes CA1 calcium imaging in rats an ideal method by which to study spatial navigation and learning over days, including mechanisms behind memory consolidation, spatial remapping, and planning over time.

Materials and Methods

SUBJECT DETAILS

All procedures were performed within Northwestern Institutional Animal Care and Use Committee and NIH guidelines. Five male Fischer 344 x Brown Norway rats (275g to 325g) were sourced from National Institute on Aging colony at Charles River Laboratories, injected with AAV9-GCaMP7c, implanted with a 2mm GRIN lens and run on linear maze (Figure S2). Animals were individually housed in an animal facility with a 12h light dark cycle.

METHOD DETAILS

GCaMP7s Injection and Lens Implantation

Rats were anesthetized with isoflurane (induction 4%, maintenance 1-2%). Following anesthesia, ear bars, and skull leveling, the skull was cleaned and a craniotomy site was marked above CA1 (stereotaxic coordinates Bregma AP -4.00mm, ML 3.00mm). The skull was scored around the craniotomy site using a razor blade to provide texture for future application of epoxy. A craniotomy was made with a 2mm trephine around the marked site and dura was removed with a bent 30 gage needle. A Hamilton syringe (Gastight® 1700 Series Syringes, Hamilton, Model 1705 Small RN Syringe, Volume=50 μL, Point Style=3, Gauge=22s, Needle Length=50.8 mm) loaded with AAV9-GCaMP7c (obtained from Viogene Biosciences, packaged AAV9 of pGP-AAV-syn-jGCaMP7c-WPRE, titer $1.73*10^{13}$GC/mL) was lowered straight down to about 0.2mm past the CA1 cell layer (approximate coordinates Bregma AP -4.00mm, ML 3mm, DV 2.95mm relative to skull)—this was often slightly off-center of the craniotomy. 0.6uL of virus were injected over 12 minutes using an automated stereotaxic Injector.

The syringe was then raised 0.2mm (Bregma AP -4.00mm, ML 3mm, DV 2.75mm) and another 0.6uL of virus were injected over 12 minutes (Figure 1a). The syringe was then left for 10 minutes before slowly raising to the skull. Because the previous injection was often slightly off center of the craniotomy, the process of lowering the syringe and doing two injections was repeated so that the two syringe “lowering points” were evenly spread throughout the craniotomy site. There were thus a total of

333 four injections of 0.6uL each (2.4uL total): two injections per each brain entrance site,
334 each at different depths (Figure 1a).
335 Following injection, four skull screws were screwed into the skull: one rostral to
336 bregma above the same hemisphere as the craniotomy, two between bregma and
337 lambda on the hemisphere opposite the craniotomy, and one behind lambda on the
338 hemisphere with the craniotomy. Under a dissecting microscope, tissue from the
339 craniotomy was then aspirated using a vacuum pump and 25 gage needle that had
340 been previously blunted using a Dremel drill. Tissue was quickly aspirated until the start
341 of horizontal striations could be seen in the craniotomy hole. Care was then taken to
342 "level" the hole and make sure aspiration was at an even depth. The horizontal
343 striations of the corpus callosum were then carefully and slowly aspirated until the
344 vertical striations of the alveus were visible in the entirety of the craniotomy hole (Figure
345 1b). If the aspiration hole was bleeding, a small twisted piece of gel foam was inserted
346 into the hole for approximately five minutes and then removed.
347 *Notes differentiating this method from mouse Ca2+ imaging: We found the best*
348 *AAV for expression in rats was AAV9. Because of rat's lower seizure threshold and,*
349 *anecdotally noted, lower GCaMP expression than in mice, four injection sites appear*
350 *both necessary and sufficient for ideal GCaMP expression. The injection volumes are*
351 *much larger than those used in mice [14, 15], which is made possible due to the larger*
352 *hippocampal area and the technique of injecting below the CA1 cell layer, instead of on*
353 *it. Unlike in mice, where just the cortex or most dorsal part of the corpus callosum is*
354 *aspirated [15, 100], it is important that the entire corpus callosum be completely*
355 *aspirated in order to get very close to the alveus.*
356 A 2mm GRIN lens (obtained from Go!Foton, CLH lens, 2.00mm diameter, 0.448
357 pitch, working distance 0.30mm, 550nm wavelength) was then held on the end of a
358 pipette using suction from the vacuum pump. The pipette was placed in the stereotaxic
359 instrument which was zero-ed with the bottom of the lens on bregma. The lens was then
360 moved to the center of the craniotomy and lowered to a depth of approximately 3mm
361 from skull surface. The lens was then fixed in place with UV curing epoxy and the
362 vacuum pump was turned off and the pipette holding the lens removed. The epoxied

363 lens was then secured to the skull screws using dental acrylic. Animals were then given
364 buprenorphine (0.05mg/kg) and 20mL saline, taken off anesthesia, and allowed to
365 recover in a clean cage place upon a heat pad.

366 *Notes differentiating this method from mouse Ca2+ imaging: A much larger lens*
367 *(2mm diameter as opposed to 0.5mm or 1.0mm diameter) lens can be used in rats due*
368 *to their larger size. Of high importance: in order to be as close to the CA1 layer as*
369 *possible, the lens is inserted further down (about .5mm) lower than the cell layer. This*
370 *serves, presumably, to compress the alveus to allow for in focus imaging of the CA1.*
371 *We had zero visualization of cells unless the lens was deeply inserted. Additionally,*
372 *unlike in mouse implantation surgeries, did not have success using meloxicam after*
373 *surgery as it appeared to cause excessive bleeding around the lens.*

374 Four to six weeks after surgery, animals were again anesthetized with isoflurane
375 and checked for cells expressing GCaMP. If expression was seen, the animal's lens
376 was base-plated. The baseplate was attached using UV-curing epoxy and dental
377 acrylic.

378 *Notes differentiating this method from mouse Ca2+ imaging: During base plating,*
379 *is gets progressively harder to see cells the longer the animal is under anesthesia.*
380 *Additionally, while a few cells will appear to be bright circles in the captured image, cells*
381 *do not appear to be flashing at all while the rat is under isoflorane, even after a tail pinch*
382 *or loud noise (techniques often used to incite a calcium during mouse base plating). We*
383 *recommend focusing on the bright, not flashing cells while base plating. The entire field*
384 *of view should become progressively brighter as the animal wakes up. We recommend*
385 *not imaging for experiments within 24 hours of isoflurane exposure and base plating.*
386

387 **Behavioral Training**

388 Prior to training, animals were food deprived to 85% body weight and maintained
389 at this weight throughout the experiment. Implanted animals were trained on a 2.64m
390 Med Associates linear track with pellet dispensers at either end. Animals learned to run
391 back and forth between the sides of the track and received a grain pellet at alternate
392 ends. Each pellet received was considered a trial. The fasted animals were able to

393 achieve over 120 trials in 30 minutes. (Animal were fed after daily training to maintain
394 weight.) Six sessions were selected for analysis for each animal, with first and last
395 recorded sessions automatically included. When not being run, animals were housed in
396 individual cages with a 12hr light- 12hr dark light cycle.
397
398 **Calcium Imaging**
399 One photon calcium imaging was done using UCLA V4 Miniscopes [101, 102],
400 assembled with standard lens configurations (two 3mm diameter, 6mm FL achromat
401 lens used in the objective module and one 4 mm diameter, 10mm FL achromat lens
402 used in the emission module). We tested Ca2+ recording when one of the objective
403 module lenses was replaced by a 3mm diameter, 9mm FL achromat lens, but no
404 improvement in cell visualization was noted. Gain was set at high and Miniscope LED
405 intensity varied between 10 and 38.
406 *Notes differentiating this method from mouse Ca2+ imaging: Base fluorescence*
407 *appears lower in rats as compared to mice. While we have been advised that, using*
408 *Miniscopes, gain can often be on "low" for mouse imaging, we found it necessary to*
409 *have gain on "high" to visualize the highest number of cells.*
410
411 **GCaMP Visualization in Slice**
412 Following conclusion of the study, animals were anesthetized and perfused with
413 PBS then 10% formalin. The brain was then sliced into 60 micron coronal sections,
414 mounted, let dry, and coverslipped with Vectashield. Sections were then imaged with a
415 confocal microscope.
416
417
418 ***QUANTIFICATION AND STATISTICAL ANALYSIS***
419 Means are expressed as mean +- the standard deviation. All analysis code is available
420 at https://github.com/hsw28/ca_imaging.
421
422 **Position and speed analysis**

423 Position was sampled by an overhead camera at 30Hz. Position tracking was
424 done post-recording using Bonsai [103]. Speed was determined by taking the
425 hypotenuse of the coordinates of the point one before and one after the time point of
426 interest. Speed was then smoothed using a Gaussian kernel of 1s and speed was
427 converted from pixels/s to cm/s.
428
429 **Video pre-processing**
430 Videos were recorded with Miniscope software at 15 frames/second and 752 by
431 480 pixels. All video processing was done using the Matlab-based CIATAH software
432 [76, 77] and processing files are available at https://github.com/hsw28/ca_imaging/ .
433 Videos were down sampled in space (3x using bi-linear interpolation) and time (2x). The
434 video was normalized by subtracting the mean value of each frame from the frame.
435 Each frame was then spatially filtered (normalized) using a bandpass FFT filter (70-
436 100cycles/pixel). The video was then motion corrected to a chosen reference frame
437 using TurboReg [104]. Videos were then converted to relative florescence (dF/F_0),
438 where F_0 was the mean over the entire video.
439
440 **Cell identification**
441 Cells were first automatically identified using the Matlab-based CIATAH software
442 [76, 77], using the CNMF-E method [75]. Processing files are available at
443 https://github.com/hsw28/ca_imaging/ . Images were filtered with a gaussian kernel of
444 width 3 pixels. Neuron diameter was set at a pixel size of 13. The threshold for merging
445 neurons was set at a calcium trace correlation of 0.65, and neurons were merged if their
446 distances were smaller than 2 pixels and they had highly correlated spatial shapes
447 (correlation>0.8) and small temporal correlations (correlation <0.4).
448 All cells identified using CNMF-E were then scored as neurons or not by a
449 human scorer. Scoring was also done within the Matlab-based CIATAH software [76,
450 77] in a Matlab GUI. Human scoring was done while visualizing an activity trace,
451 average Ca2+ waveform, a cropped movie montage of the candidate cell's Ca2+
452 events, and a maximum projection of all cells on which the candidate cell was

453 highlighted. The relative fluorescence ($\Delta F/F_0$) local maxima of each identified cell were
454 considered calcium event times.
455
456 **Place cell identification**
457 Place cells were identified using two criteria. First, cells must have a mean firing
458 rate greater than 0.01Hz during periods of movement (>12cm/s) [83, 105]. Second, the
459 mutual information (MI) computed in either direction of travel must be greater than 95%
460 of MI scores computed 500 times from shuffled cells [78]. To compute MI, the track was
461 divided lengthwise into 4cm bins the firing rate of each cell and the occupancy of the
462 animal were found for each bin. Rate and occupancy were smoothed with a 2cm
463 Gaussian kernel. Mutual information was computed during periods of movement in each
464 direction of travel as follows [78, 83, 106]:
465 $P_s = calcium\ event\ probability\ in\ each\ bin$
466 $P_o = occupancy\ probability\ at\ each\ bin$
467 $p = \frac{P_s}{P_o}$
468 $M_s = \sum P_s$
469 $M_o = \sum P_o$
470 $$MI = \sum p * \log_2(\frac{p}{M_s * M_o})$$
471
472
473 **Position decoding**
474 Position was decoded using all recorded cells in a session and was decoded for
475 times when the rat was moving (velocity>12cm/s). The track was split in 10cm
476 segments and the time window of decoding was 0.5 seconds with non-overlapping time
477 bins. Decoding was done using Bayesian decoding [79].
478 $x = positions, f_i(x) = average\ firing\ rate\ per\ second\ for\ cell\ N\ at\ position\ X$
479 $n = calcium\ events\ per\ cell, n_i = number\ of\ events\ in\ time\ window$
480 $N = total\ number\ of\ cells$

481 $t = time\ window\ of\ decoding$

482 $C(t,n) = normalization\ factor\ for\ probabilities\ to\ equal\ 1$

483 $P(x|n) = odds\ of\ being\ at\ position\ x\ giving\ calcium\ events\ n$

484 $$P(x|n) = C(t,n)\left(\prod_{i=1}^{\mathrm{N}} f_i(x)^{n_i}\right)\exp\left(-t\sum_{i=1}^{\mathrm{N}} f_i(x)\right)$$

485

486 Accuracy decoding was determined by randomly shuffling firing per position bins
487 and re-decoding. The difference between actual and decoded position was then
488 determined per time bin and compared to decoded shuffled data.

489

490 **Validation across days and within session**

491 Validation was done using the Matlab-based CIATAH software [76, 77]. Videos
492 underwent 3 rounds of registration comprised of Turboreg image rotation [104]. An
493 image binarization threshold of 40% of the images' maximum value was used to remove
494 background noise and axons and dendrites. A distance threshold of a maximum of 5
495 pixels was used to match cells across sessions, with a minimum 2-D correlation
496 coefficient of 0.5. All sessions were aligned to the last recording session.

497 Photobleaching analysis was performed by computing the mean brightness for
498 each identified cell for a five-minute period towards the beginning of the session and
499 comparing it to the brightness for a five-minute period towards the end of the session.
500 (Mean brightness was the mean $\Delta F/F_0$ for each cell over the time period). The sampling
501 periods were separated from session start and end by five minutes to avoid behavioral
502 correlates related to starting and finishing the task period (Figure 5b). Results from
503 beginning to end of session were compared with a paired T-test. To normalize
504 brightness by the number of calcium events that occurred in each five-minute time
505 period, the number of events per cell were counted for the period. The mean
506 fluorescence for the period for that cell was then divided by the mean number of events.

507

508

509

510

511

512

513

514 **Figure captions**

515

516 **Figure 1:** GCaMP is expressed in the CA1 cell layer of rat hippocampus

517 a. Diagram showing injection locations of AAV9-Syn-GCaMP7c, right below the
518 CA1 cell layer. There are four total injection sites, with 0.6uL injected at each
519 site. (CC = corpus callosum, DG = dentate gyrus)

520 b. Diagram showing level of aspiration in brain tissue. The entire corpus
521 callosum is aspirated until the vertical striations of the alveus are visible.

522 c. GCaMP expression in the hippocampus, taken with a confocal microscope.
523 The CA1 cell layer is labeled.

524

525 **Figure 2:** Hundreds of cells can be captured in a single Ca2+ imaging session

526 a. Examples of data from two (top and bottom rows) recording sessions. First
527 column: example image from pre-processing. Second column: image post-
528 processing (see materials and methods). Third column: all cell extractions,
529 prior to manual cell sorting. Fourth column: post processing image overlayed
530 with cell outlines identified after manual sorting.

531 b. Example traces from 15 cells taken during 124 seconds of calcium imaging.

532 c. Raster plot of cell firing during linear track running. Top: the animal's speed.
533 Bottom: raster of peak calcium transients of 352 identified cells.

534 d. Number of cells imaged per session for each rat. Dotted red line indicates the
535 average for each animal.

536

537 **Figure 3:** A high percentage of place cells are recorded on the linear track using Ca2+
538 imaging

539 a. Graph showing the percentage of place cells (out of total recorded cells with a
540 firing rate >0.1Hz during movement) per session for each rat. Dotted red line
541 indicates the average for each animal.

542 b. Nine example place cells. A firing rate map in both directions of travel is
543 provided for each cell, with the top map corresponding with running to the

544 right, and the bottom map corresponding with running to the left. Note the
545 colorbar scales may be different for each direction of travel. The difference in
546 mutual information scores between the cell and the top 95% of shuffled data
547 (actual MI-shuffled MI) is indicated in the left corner. If the actual MI was
548 greater than 95% of shuffled data, the number is printed in bold white.
549 c. Distribution of directional mutual information scores after shuffling cells seen
550 in figure 3b. Event data was shuffled 500 times and the top 95% of mutual
551 information scores were determined from shuffled data (red dotted line). If the
552 actual mutual information score (green line) was greater than the upper 95%
553 MI score of shuffled data, the cell was considered to be a place cell.
554
555 **Figure 4:** Place cells are sufficient to decode the animal's position
556 a. Four decoding examples as the animal traverses the track. Black line
557 indicates the animal's actual position, with the stars indicated sample point.
558 The colored circles connected by the red line indicate decoded position. The
559 color of the circles indicates decoding certainty.
560 b. Same as A but decoding is using shuffled units. Decoding is much less
561 accurate using shuffled data.
562
563 **Figure 5:** Individual cells can be maintained across session and within session.
564 a. Cells can be maintained across sessions weeks apart. Examples from two
565 animals of data taken on the first and final days of recording. Cells are color-
566 matched from the first to last day. Cells in gray represent cells with no
567 matches between the two days. Of note, these recordings were prioritized for
568 cell number as proof of concept rather than maintaining the same landmarks
569 (such as blood vessels) across days.
570 b. Top: method for comparing calcium signal brightness across session. The
571 mean brightness for each identified cell was computed for a five minute
572 period towards the beginning of the session and compared to the mean
573 brightness for a five minute period towards the end of the session. The

sampling periods were separated from session start and end by five minutes to avoid psychological or behavioral correlates related to starting and finishing the task period. Bottom: Histogram of change in fluorescence from starting to ending, for all 5751 recorded cells (mean change = .008, median change = $-2.01*10^{-4}$), There was no consistent change in fluorescence when examining at the cell level. Examining by groups of cells in each session, in 22 out of the 24 sessions, the end mean fluorescence of each cell was not less than the starting mean fluorescence (one-tailed paired t-test, $p>0.05$), and for 6 of these sessions, the end mean fluorescence was actually greater than the starting fluorescence (one-tailed paired t-test, $p<0.05$). Two sessions (8% of sessions) showed a decrease in fluorescence (one-tailed paired t-test, $t(368)=2.47$, $p<0.01$, and $t(231)=1.98$, $p<0.05$). For ease of viewing, outliers were removed from visualization (but not analysis).

c. To control for the number of calcium events, we normalized the fluorescence in each five-minute period by the number of events in the period and then found the change in fluorescence from beginning to end of session (mean change = $-1.77*10^{-4}$, median change = $-5.7*10^{-8}$). Even after normalization, still only two sessions (although a different two) showed a decrease in fluorescence from the start period to the end period (one-tailed paired t-test, $t(226)=1.7$, $p=0.04$, and $t(349)=2.1$, $p=0.02$), while three sessions showed an increase (one-tailed paired t-test, $t(123)=-1.9$; $p=0.03$, $t(173)=-3.0$, $p<0.005$; $t(166)=-4.0$, $p<0.00005$). There was therefore no consistent loss of fluorescence within each session. For ease of viewing, outliers were removed from visualization (but not analysis).

Figure S1: Animals ran on a linear track.

a. Diagram of linear track. The animal would run back and forth between the two sides to receive a pellet reward
b. Trace of animal position over one session

Figure S2: Percentage of cells that are place cells without using a firing rate cutoff. Percent is indicated for each day of recording, by animal. Red dotted line indicates the average for the animal.

Acknowledgements

We would like to thank all members of the Disterhoft lab, especially Matthew Oh, Craig Weiss, and Kent Park. We would also like to thank the Miniscope team, in particular Daniel Aharoni and Federico Sangiuliano Jimka. We additionally thank Biafra Ahanonu for assistance with CIATAH, Amy Christensen for providing advice during imaging setup, David Wirtshafter for discussion and editing help, and Drew Ames for consultation on figures.

Funding Disclosure

This work was supported by an NIA T32 (T32-AG020506/AG/NIA), an NIA R37 (R37-AG008796/AG/NIA) and an NINDS R01 (R01 NS113804/NS/NINDS).

Competing Interests

The authors declare no competing interests.

Related Manuscripts

Authors do not have a related or duplicate manuscript under consideration (or accepted) for publication elsewhere.

Citations

1. Grienberger C, Konnerth A. Imaging calcium in neurons. Neuron. 2012;73(5):862-85. doi: 10.1016/j.neuron.2012.02.011. PubMed PMID: 22405199.
2. Aharoni D, Hoogland TM. Circuit Investigations With Open-Source Miniaturized Microscopes: Past, Present and Future. Frontiers in cellular neuroscience. 2019;13:141. doi: 10.3389/fncel.2019.00141. PubMed PMID: 31024265; PubMed Central PMCID: PMCPMC6461004.
3. Aharoni D, Khakh BS, Silva AJ, Golshani P. All the light that we can see: a new era in miniaturized microscopy. Nat Methods. 2019;16(1):11-3. doi: 10.1038/s41592-018-0266-x. PubMed PMID: 30573833.
4. Rickgauer JP, Deisseroth K, Tank DW. Simultaneous cellular-resolution optical perturbation and imaging of place cell firing fields. Nat Neurosci. 2014;17(12):1816-24. doi: 10.1038/nn.3866. PubMed PMID: 25402854; PubMed Central PMCID: PMCPMC4459599.
5. Resendez SL, Jennings JH, Ung RL, Namboodiri VM, Zhou ZC, Otis JM, et al. Visualization of cortical, subcortical and deep brain neural circuit dynamics during naturalistic mammalian behavior with head-mounted microscopes and chronically implanted lenses. Nature protocols. 2016;11(3):566-97. Epub 2016/02/26. doi: 10.1038/nprot.2016.021. PubMed PMID: 26914316; PubMed Central PMCID: PMCPMC5239057.
6. Grienberger C, Konnerth A. Imaging calcium in neurons. Neuron. 2012;73(5):862-85.
7. Hamel EJ, Grewe BF, Parker JG, Schnitzer MJ. Cellular level brain imaging in behaving mammals: an engineering approach. Neuron. 2015;86(1):140-59. Epub 2015/04/10. doi: 10.1016/j.neuron.2015.03.055. PubMed PMID: 25856491; PubMed Central PMCID: PMCPMC5758309.
8. Zhou H, Neville KR, Goldstein N, Kabu S, Kausar N, Ye R, et al. Cholinergic modulation of hippocampal calcium activity across the sleep-wake cycle. eLife. 2019;8. Epub 2019/03/08. doi: 10.7554/eLife.39777. PubMed PMID: 30843520; PubMed Central PMCID: PMCPMC6435325.
9. Sheintuch L, Rubin A, Brande-Eilat N, Geva N, Sadeh N, Pinchasof O, et al. Tracking the Same Neurons across Multiple Days in Ca(2+) Imaging Data. Cell reports. 2017;21(4):1102-15. doi: 10.1016/j.celrep.2017.10.013. PubMed PMID: 29069591; PubMed Central PMCID: PMCPMC5670033.
10. Hainmueller T, Bartos M. Parallel emergence of stable and dynamic memory engrams in the hippocampus. Nature. 2018;558(7709):292-6. doi: 10.1038/s41586-018-0191-2. PubMed PMID: 29875406.
11. Dombeck DA, Harvey CD, Tian L, Looger LL, Tank DW. Functional imaging of hippocampal place cells at cellular resolution during virtual navigation. Nat Neurosci. 2010;13(11):1433-40. doi: 10.1038/nn.2648. PubMed PMID: 20890294; PubMed Central PMCID: PMCPMC2967725.
12. Kinsky NR, Mau W, Sullivan DW, Levy SJ, Ruesch EA, Hasselmo ME. Trajectory-modulated hippocampal neurons persist throughout memory-guided navigation. Nature communications. 2020;11(1):2443. Epub 2020/05/18. doi: 10.1038/s41467-020-16226-4. PubMed PMID: 32415083; PubMed Central PMCID: PMCPMC7229120.

13. Sheintuch L, Geva N, Baumer H, Rechavi Y, Rubin A, Ziv Y. Multiple Maps of the Same Spatial Context Can Stably Coexist in the Mouse Hippocampus. Current biology : CB. 2020;30(8):1467-76 e6. Epub 2020/03/30. doi: 10.1016/j.cub.2020.02.018. PubMed PMID: 32220328.

14. Ziv Y, Burns LD, Cocker ED, Hamel EO, Ghosh KK, Kitch LJ, et al. Long-term dynamics of CA1 hippocampal place codes. Nat Neurosci. 2013;16(3):264-6. Epub 2013/02/12. doi: 10.1038/nn.3329. PubMed PMID: 23396101; PubMed Central PMCID: PMCPMC3784308.

15. Cai DJ, Aharoni D, Shuman T, Shobe J, Biane J, Song W, et al. A shared neural ensemble links distinct contextual memories encoded close in time. Nature. 2016;534(7605):115-8. Epub 2016/06/03. doi: 10.1038/nature17955. PubMed PMID: 27251287; PubMed Central PMCID: PMCPMC5063500.

16. Jimenez JC, Berry JE, Lim SC, Ong SK, Kheirbek MA, Hen R. Contextual fear memory retrieval by correlated ensembles of ventral CA1 neurons. Nature communications. 2020;11(1):3492. Epub 2020/07/15. doi: 10.1038/s41467-020-17270-w. PubMed PMID: 32661319; PubMed Central PMCID: PMCPMC7359370.

17. Zhang X, Li B. Population coding of valence in the basolateral amygdala. Nature communications. 2018;9(1):5195. Epub 2018/12/07. doi: 10.1038/s41467-018-07679-9. PubMed PMID: 30518754; PubMed Central PMCID: PMCPMC6281657.

18. Shuman T, Aharoni D, Cai DJ, Lee CR, Chavlis S, Page-Harley L, et al. Breakdown of spatial coding and interneuron synchronization in epileptic mice. Nat Neurosci. 2020;23(2):229-38. Epub 2020/01/08. doi: 10.1038/s41593-019-0559-0. PubMed PMID: 31907437; PubMed Central PMCID: PMCPMC7259114.

19. Shin JH, Song M, Paik SB, Jung MW. Spatial organization of functional clusters representing reward and movement information in the striatal direct and indirect pathways. Proc Natl Acad Sci U S A. 2020;117(43):27004-15. Epub 2020/10/16. doi: 10.1073/pnas.2010361117. PubMed PMID: 33055217; PubMed Central PMCID: PMCPMC7604453.

20. Wang X, Liu Y, Li X, Zhang Z, Yang H, Zhang Y, et al. Deconstruction of Corticospinal Circuits for Goal-Directed Motor Skills. Cell. 2017;171(2):440-55 e14. Epub 2017/09/26. doi: 10.1016/j.cell.2017.08.014. PubMed PMID: 28942925; PubMed Central PMCID: PMCPMC5679421.

21. Klaus A, Martins GJ, Paixao VB, Zhou P, Paninski L, Costa RM. The Spatiotemporal Organization of the Striatum Encodes Action Space. Neuron. 2017;95(5):1171-80 e7. Epub 2017/09/01. doi: 10.1016/j.neuron.2017.08.015. PubMed PMID: 28858619; PubMed Central PMCID: PMCPMC5584673.

22. Guo W, Zhang JJ, Newman JP, Wilson MA. Latent learning drives sleep-dependent plasticity in distinct CA1 subpopulations. bioRxiv. 2020:2020.02.27.967794. doi: 10.1101/2020.02.27.967794.

23. O'Keefe J. Place units in the hippocampus of the freely moving rat. Exp Neurol. 1976;51(1):78-109. Epub 1976/04/01. PubMed PMID: 1261644.

24. Wilson MA, McNaughton BL. Dynamics of the hippocampal ensemble code for space. Science. 1993;261(5124):1055-8. Epub 1993/08/20. PubMed PMID: 8351520.

25. Leutgeb S, Leutgeb JK, Treves A, Moser MB, Moser EI. Distinct ensemble codes in hippocampal areas CA3 and CA1. Science. 2004;305(5688):1295-8. Epub 2004/07/24. doi: 10.1126/science.1100265
1100265 [pii]. PubMed PMID: 15272123.
26. McEchron MD, Disterhoft JF. Hippocampal encoding of non-spatial trace conditioning. Hippocampus. 1999;9(4):385-96. doi: 10.1002/(SICI)1098-1063(1999)9:4<385::AID-HIPO5>3.0.CO;2-K. PubMed PMID: 10495020.
27. Schimanski LA, Lipa P, Barnes CA. Tracking the course of hippocampal representations during learning: when is the map required? J Neurosci. 2013;33(7):3094-106. doi: 10.1523/JNEUROSCI.1348-12.2013. PubMed PMID: 23407964; PubMed Central PMCID: PMCPMC3700421.
28. Stefanini F, Kushnir L, Jimenez JC, Jennings JH, Woods NI, Stuber GD, et al. A Distributed Neural Code in the Dentate Gyrus and in CA1. Neuron. 2020;107(4):703-16 e4. Epub 2020/06/11. doi: 10.1016/j.neuron.2020.05.022. PubMed PMID: 32521223; PubMed Central PMCID: PMCPMC7442694.
29. Scoville WB, Milner B. Loss of recent memory after bilateral hippocampal lesions. Journal of neurology, neurosurgery, and psychiatry. 1957;20(1):11-21. Epub 1957/02/01. PubMed PMID: 13406589; PubMed Central PMCID: PMC497229.
30. Squire LR. Memory and the hippocampus: a synthesis from findings with rats, monkeys, and humans. Psychol Rev. 1992;99(2):195-231. Epub 1992/04/01. PubMed PMID: 1594723.
31. Hasselmo ME, McClelland JL. Neural models of memory. Curr Opin Neurobiol. 1999;9(2):184-8. Epub 1999/05/14. doi: S0959-4388(99)80025-7 [pii]. PubMed PMID: 10322183.
32. Ferbinteanu J, Shapiro ML. Prospective and retrospective memory coding in the hippocampus. Neuron. 2003;40(6):1227-39. Epub 2003/12/23. doi: S0896627303007529 [pii]. PubMed PMID: 14687555.
33. Smith DM, Mizumori SJ. Hippocampal place cells, context, and episodic memory. Hippocampus. 2006;16(9):716-29. Epub 2006/08/10. doi: 10.1002/hipo.20208. PubMed PMID: 16897724.
34. Vann SD. Dismantling the Papez circuit for memory in rats. eLife. 2013;2:e00736. Epub 2013/06/28. doi: 10.7554/eLife.00736. PubMed PMID: 23805381; PubMed Central PMCID: PMC3691571.
35. Josselyn SA, Tonegawa S. Memory engrams: Recalling the past and imagining the future. Science. 2020;367(6473). Epub 2020/01/04. doi: 10.1126/science.aaw4325. PubMed PMID: 31896692.
36. Eichenbaum H, Dudchenko P, Wood E, Shapiro M, Tanila H. The hippocampus, memory, and place cells: is it spatial memory or a memory space? Neuron. 1999;23(2):209-26. Epub 1999/07/10. doi: S0896-6273(00)80773-4 [pii]. PubMed PMID: 10399928.
37. Ferbinteanu J, Kennedy PJ, Shapiro ML. Episodic memory—from brain to mind. Hippocampus. 2006;16(9):691-703.
38. McNaughton BL, Battaglia FP, Jensen O, Moser EI, Moser MB. Path integration and the neural basis of the 'cognitive map'. Nat Rev Neurosci. 2006;7(8):663-78. Epub 2006/07/22. doi: nrn1932 [pii]
10.1038/nrn1932. PubMed PMID: 16858394.

39. Foster DJ, Knierim JJ. Sequence learning and the role of the hippocampus in rodent navigation. Curr Opin Neurobiol. 2012;22(2):294-300. Epub 2012/01/10. doi: 10.1016/j.conb.2011.12.005
S0959-4388(11)00223-6 [pii]. PubMed PMID: 22226994.
40. Foster DJ, Morris RG, Dayan P. A model of hippocampally dependent navigation, using the temporal difference learning rule. Hippocampus. 2000;10(1):1-16. Epub 2000/03/08. doi: 10.1002/(SICI)1098-1063(2000)10:1<1::AID-HIPO1>3.0.CO;2-1. PubMed PMID: 10706212.
41. Avigan PD, Cammack K, Shapiro ML. Flexible spatial learning requires both the dorsal and ventral hippocampus and their functional interactions with the prefrontal cortex. Hippocampus. 2020;30(7):733-44.
42. Moser EI, Moser M-B, McNaughton BL. Spatial representation in the hippocampal formation: a history. Nature neuroscience. 2017;20(11):1448-64.
43. Rosenzweig ES, Redish AD, McNaughton BL, Barnes CA. Hippocampal map realignment and spatial learning. Nature neuroscience. 2003;6(6):609-15.
44. Moyer JR, Jr., Deyo RA, Disterhoft JF. Hippocampectomy disrupts trace eye-blink conditioning in rabbits. Behav Neurosci. 1990;104(2):243-52. PubMed PMID: 2346619.
45. Andrzejewski ME, Ryals C. Dissociable hippocampal and amygdalar D1-like receptor contribution to discriminated Pavlovian conditioned approach learning. Behav Brain Res. 2016;299:111-21. doi: 10.1016/j.bbr.2015.11.034. PubMed PMID: 26632336; PubMed Central PMCID: PMCPMC4866504.
46. Ito R, Everitt BJ, Robbins TW. The hippocampus and appetitive Pavlovian conditioning: effects of excitotoxic hippocampal lesions on conditioned locomotor activity and autoshaping. Hippocampus. 2005;15(6):713-21. doi: 10.1002/hipo.20094. PubMed PMID: 15906393.
47. Chan KH, Morell JR, Jarrard LE, Davidson TL. Reconsideration of the role of the hippocampus in learned inhibition. Behav Brain Res. 2001;119(2):111-30. PubMed PMID: 11165328.
48. Pritchard A, Hornung R, Kramer PR. Measuring calcium activity within individual neurons within the rat thalamus. MethodsX. 2021;8:101273.
49. Anner P, Passecker J, Klausberger T, Dorffner G. Ca2+ imaging of neurons in freely moving rats with automatic post hoc histological identification. Journal of neuroscience methods. 2020;341:108765.
50. Scott BB, Thiberge SY, Guo C, Tervo DGR, Brody CD, Karpova AY, et al. Imaging cortical dynamics in GCaMP transgenic rats with a head-mounted widefield macroscope. Neuron. 2018;100(5):1045-58. e5.
51. Hart EE, Blair GJ, O'Dell TJ, Blair HT, Izquierdo A. Chemogenetic modulation and single-photon calcium imaging in anterior cingulate cortex reveal a mechanism for effort-based decisions. Journal of Neuroscience. 2020;40(29):5628-43.
52. Swanson L. Brain maps: structure of the rat brain: Gulf Professional Publishing; 2004.
53. Franklin KBJ, Paxinos G. Paxinos and Franklin's The mouse brain in stereotaxic coordinates2013.
54. Routh BN, Johnston D, Harris K, Chitwood RA. Anatomical and electrophysiological comparison of CA1 pyramidal neurons of the rat and mouse. Journal of neurophysiology. 2009;102(4):2288-302.

802 55. Whishaw IQ. A comparison of rats and mice in a swimming pool place task and matching
803 to place task: some surprising differences. Physiol Behav. 1995;58(4):687-93. Epub 1995/10/01.
804 doi: 10.1016/0031-9384(95)00110-5. PubMed PMID: 8559777.
805 56. Frick KM, Stillner ET, Berger-Sweeney J. Mice are not little rats: species differences in a
806 one-day water maze task. Neuroreport. 2000;11(16):3461-5. Epub 2000/11/30. doi:
807 10.1097/00001756-200011090-00013. PubMed PMID: 11095500.
808 57. Rosenfeld CS, Ferguson SA. Barnes maze testing strategies with small and large rodent
809 models. J Vis Exp. 2014;(84):e51194. Epub 2014/03/19. doi: 10.3791/51194. PubMed PMID:
810 24637673; PubMed Central PMCID: PMCPMC4140524.
811 58. Cressant A, Besson M, Suarez S, Cormier A, Granon S. Spatial learning in Long-Evans
812 Hooded rats and C57BL/6J mice: different strategies for different performance. Behav Brain
813 Res. 2007;177(1):22-9. Epub 2006/12/13. doi: 10.1016/j.bbr.2006.11.010. PubMed PMID:
814 17157932.
815 59. Hok V, Poucet B, Duvelle É, Save É, Sargolini F. Spatial cognition in mice and rats:
816 similarities and differences in brain and behavior. Wiley Interdisciplinary Reviews: Cognitive
817 Science. 2016;7(6):406-21.
818 60. Whishaw IQ, Metz GA, Kolb B, Pellis SM. Accelerated nervous system development
819 contributes to behavioral efficiency in the laboratory mouse: a behavioral review and
820 theoretical proposal. Developmental Psychobiology: The Journal of the International Society for
821 Developmental Psychobiology. 2001;39(3):151-70.
822 61. Vengeliene V, Bilbao A, Spanagel R. The alcohol deprivation effect model for studying
823 relapse behavior: a comparison between rats and mice. Alcohol. 2014;48(3):313-20. Epub
824 2014/05/09. doi: 10.1016/j.alcohol.2014.03.002. PubMed PMID: 24811155.
825 62. Carter CS, Richardson A, Huffman DM, Austad S. Bring Back the Rat! J Gerontol A Biol Sci
826 Med Sci. 2020;75(3):405-15. Epub 2020/01/03. doi: 10.1093/gerona/glz298. PubMed PMID:
827 31894235; PubMed Central PMCID: PMCPMC7021637.
828 63. Ellenbroek B, Youn J. Rodent models in neuroscience research: is it a rat race? Dis Model
829 Mech. 2016;9(10):1079-87. Epub 2016/10/14. doi: 10.1242/dmm.026120. PubMed PMID:
830 27736744; PubMed Central PMCID: PMCPMC5087838.
831 64. Iannaccone PM, Jacob HJ. Rats! Dis Model Mech. 2009;2(5-6):206-10. Epub 2009/05/02.
832 doi: 10.1242/dmm.002733. PubMed PMID: 19407324; PubMed Central PMCID:
833 PMCPMC2675817.
834 65. Buerge T, Weiss T. Handling and Restraint. In: Hedrich HJ, Bullock G, editors. The
835 Laboratory Mouse (Handbook of Experimental Animals): Elsevier; 2004. p. 517-26.
836 66. Voigts J, Newman JP, Wilson MA, Harnett MT. An easy-to-assemble, robust, and
837 lightweight drive implant for chronic tetrode recordings in freely moving animals. J Neural Eng.
838 2020;17(2):026044. Epub 2020/02/20. doi: 10.1088/1741-2552/ab77f9. PubMed PMID:
839 32074511.
840 67. Voigts J, Siegle JH, Pritchett DL, Moore CI. The flexDrive: an ultra-light implant for optical
841 control and highly parallel chronic recording of neuronal ensembles in freely moving mice.
842 Front Syst Neurosci. 2013;7:8. Epub 2013/05/30. doi: 10.3389/fnsys.2013.00008. PubMed
843 PMID: 23717267; PubMed Central PMCID: PMCPMC3652307.

844 68. Bolkvadze T, Pitkanen A. Development of post-traumatic epilepsy after controlled
845 cortical impact and lateral fluid-percussion-induced brain injury in the mouse. J Neurotrauma.
846 2012;29(5):789-812. Epub 2011/10/26. doi: 10.1089/neu.2011.1954. PubMed PMID: 22023672.
847 69. Hunt RF, Scheff SW, Smith BN. Posttraumatic epilepsy after controlled cortical impact
848 injury in mice. Exp Neurol. 2009;215(2):243-52. Epub 2008/11/18. doi:
849 10.1016/j.expneurol.2008.10.005. PubMed PMID: 19013458; PubMed Central PMCID:
850 PMCPMC4694635.
851 70. Hunt RF, Scheff SW, Smith BN. Regionally localized recurrent excitation in the dentate
852 gyrus of a cortical contusion model of posttraumatic epilepsy. J Neurophysiol.
853 2010;103(3):1490-500. Epub 2010/01/22. doi: 10.1152/jn.00957.2009. PubMed PMID:
854 20089815; PubMed Central PMCID: PMCPMC2887624.
855 71. Steinmetz NA, Buetfering C, Lecoq J, Lee CR, Peters AJ, Jacobs EAK, et al. Aberrant
856 Cortical Activity in Multiple GCaMP6-Expressing Transgenic Mouse Lines. eNeuro. 2017;4(5).
857 Epub 2017/09/22. doi: 10.1523/ENEURO.0207-17.2017. PubMed PMID: 28932809; PubMed
858 Central PMCID: PMCPMC5604087.
859 72. Yang Y, Liu N, He Y, Liu Y, Ge L, Zou L, et al. Improved calcium sensor GCaMP-X
860 overcomes the calcium channel perturbations induced by the calmodulin in GCaMP. Nature
861 communications. 2018;9(1):1504. Epub 2018/04/19. doi: 10.1038/s41467-018-03719-6.
862 PubMed PMID: 29666364; PubMed Central PMCID: PMCPMC5904127.
863 73. Tian L, Hires SA, Mao T, Huber D, Chiappe ME, Chalasani SH, et al. Imaging neural
864 activity in worms, flies and mice with improved GCaMP calcium indicators. Nat Methods.
865 2009;6(12):875-81. Epub 2009/11/10. doi: 10.1038/nmeth.1398. PubMed PMID: 19898485;
866 PubMed Central PMCID: PMCPMC2858873.
867 74. Nathanson JL, Yanagawa Y, Obata K, Callaway EM. Preferential labeling of inhibitory and
868 excitatory cortical neurons by endogenous tropism of adeno-associated virus and lentivirus
869 vectors. Neuroscience. 2009;161(2):441-50. Epub 2009/03/26. doi:
870 10.1016/j.neuroscience.2009.03.032. PubMed PMID: 19318117; PubMed Central PMCID:
871 PMCPMC2728494.
872 75. Zhou P, Resendez SL, Rodriguez-Romaguera J, Jimenez JC, Neufeld SQ, Giovannucci A, et
873 al. Efficient and accurate extraction of in vivo calcium signals from microendoscopic video data.
874 eLife. 2018;7. Epub 2018/02/23. doi: 10.7554/eLife.28728. PubMed PMID: 29469809; PubMed
875 Central PMCID: PMCPMC5871355.
876 76. Ahanonu B. CIAtah: a software package for analyzing one- and two-photon calcium
877 imaging datasets. v1.0.0 ed: Zenodo; 2018.
878 77. Corder G, Ahanonu B, Grewe BF, Wang D, Schnitzer MJ, Scherrer G. An amygdalar neural
879 ensemble that encodes the unpleasantness of pain. Science. 2019;363(6424):276-81. Epub
880 2019/01/19. doi: 10.1126/science.aap8586. PubMed PMID: 30655440; PubMed Central PMCID:
881 PMCPMC6450685.
882 78. Kinsky NR, Sullivan DW, Mau W, Hasselmo ME, Eichenbaum HB. Hippocampal Place
883 Fields Maintain a Coherent and Flexible Map across Long Timescales. Current biology : CB.
884 2018;28(22):3578-88 e6. Epub 2018/11/06. doi: 10.1016/j.cub.2018.09.037. PubMed PMID:
885 30393037; PubMed Central PMCID: PMCPMC6331214.

79. Zhang K, Ginzburg I, McNaughton BL, Sejnowski TJ. Interpreting neuronal population activity by reconstruction: unified framework with application to hippocampal place cells. J Neurophysiol. 1998;79(2):1017-44. doi: 10.1152/jn.1998.79.2.1017. PubMed PMID: 9463459.
80. Li P, Geng X, Jiang H, Caccavano A, Vicini S, Wu JY. Measuring Sharp Waves and Oscillatory Population Activity With the Genetically Encoded Calcium Indicator GCaMP6f. Frontiers in cellular neuroscience. 2019;13:274. Epub 2019/07/06. doi: 10.3389/fncel.2019.00274. PubMed PMID: 31275115; PubMed Central PMCID: PMCPMC6593119.
81. Stefanini F, Kushnir L, Jimenez JC, Jennings JH, Woods NI, Stuber GD, et al. A distributed neural code in the dentate gyrus and in CA1. Neuron. 2020;107(4):703-16. e4.
82. Mou X, Cheng J, Yu YS, Kee SE, Ji D. Comparing mouse and rat hippocampal place cell activities and firing sequences in the same environments. Frontiers in cellular neuroscience. 2018;12:332.
83. Wirtshafter HS, Wilson MA. Differences in reward biased spatial representations in the lateral septum and hippocampus. eLife. 2020;9. Epub 2020/05/27. doi: 10.7554/eLife.55252. PubMed Central PMCID: PMCPMC7274787.
84. Fenton AA, Kao H-Y, Neymotin SA, Olypher A, Vayntrub Y, Lytton WW, et al. Unmasking the CA1 ensemble place code by exposures to small and large environments: more place cells and multiple, irregularly arranged, and expanded place fields in the larger space. Journal of Neuroscience. 2008;28(44):11250-62.
85. Markus EJ, Barnes CA, McNaughton BL, Gladden VL, Skaggs WE. Spatial information content and reliability of hippocampal CA1 neurons: effects of visual input. Hippocampus. 1994;4(4):410-21.
86. Ego-Stengel V, Wilson MA. Spatial selectivity and theta phase precession in CA1 interneurons. Hippocampus. 2007;17(2):161-74. doi: 10.1002/hipo.20253. PubMed PMID: 17183531.
87. Huang L, Ledochowitsch P, Knoblich U, Lecoq J, Murphy GJ, Reid RC, et al. Relationship between simultaneously recorded spiking activity and fluorescence signal in GCaMP6 transgenic mice. eLife. 2021;10:e51675.
88. Delon A, Usson Y, Derouard J, Biben T, Souchier C. Continuous photobleaching in vesicles and living cells: a measure of diffusion and compartmentation. Biophys J. 2006;90(7):2548-62. Epub 2006/01/24. doi: 10.1529/biophysj.105.069815. PubMed PMID: 16428281; PubMed Central PMCID: PMCPMC1403194.
89. Buzsaki G. Two-stage model of memory trace formation: a role for "noisy" brain states. Neuroscience. 1989;31(3):551-70. Epub 1989/01/01. doi: 0306-4522(89)90423-5 [pii]. PubMed PMID: 2687720.
90. Colgin LL. Mechanisms and functions of theta rhythms. Annu Rev Neurosci. 2013;36:295-312. doi: 10.1146/annurev-neuro-062012-170330. PubMed PMID: 23724998.
91. Hasselmo ME. What is the function of hippocampal theta rhythm?--Linking behavioral data to phasic properties of field potential and unit recording data. Hippocampus. 2005;15(7):936-49. doi: 10.1002/hipo.20116. PubMed PMID: 16158423.
92. Hasselmo ME, Hay J, Ilyn M, Gorchetchnikov A. Neuromodulation, theta rhythm and rat spatial navigation. Neural Netw. 2002;15(4-6):689-707. Epub 2002/10/10. doi: S0893-6080(02)00057-6 [pii]. PubMed PMID: 12371520.

93. Wikenheiser AM, Redish AD. Hippocampal theta sequences reflect current goals. Nat Neurosci. 2015;18(2):289-94. Epub 2015/01/07. doi: 10.1038/nn.3909. PubMed PMID: 25559082; PubMed Central PMCID: PMC4428659.
94. Wirtshafter HS, Wilson MA. Lateral septum as a nexus for mood, motivation, and movement. Neurosci Biobehav Rev. 2021;126:544-59. Epub 2021/04/14. doi: 10.1016/j.neubiorev.2021.03.029. PubMed PMID: 33848512.
95. Shirvalkar PR, Rapp PR, Shapiro ML. Bidirectional changes to hippocampal theta–gamma comodulation predict memory for recent spatial episodes. Proceedings of the National Academy of Sciences. 2010;107(15):7054-9.
96. Hirst WD, Abrahamsen B, Blaney FE, Calver AR, Aloj L, Price GW, et al. Differences in the central nervous system distribution and pharmacology of the mouse 5-hydroxytryptamine-6 receptor compared with rat and human receptors investigated by radioligand binding, site-directed mutagenesis, and molecular modeling. Molecular pharmacology. 2003;64(6):1295-308.
97. Snyder JS, Choe JS, Clifford MA, Jeurling SI, Hurley P, Brown A, et al. Adult-born hippocampal neurons are more numerous, faster maturing, and more involved in behavior in rats than in mice. Journal of Neuroscience. 2009;29(46):14484-95.
98. Parker CC, Chen H, Flagel SB, Geurts AM, Richards JB, Robinson TE, et al. Rats are the smart choice: rationale for a renewed focus on rats in behavioral genetics. Neuropharmacology. 2014;76:250-8.
99. Jupp B, Caprioli D, Dalley JW. Highly impulsive rats: modelling an endophenotype to determine the neurobiological, genetic and environmental mechanisms of addiction. Dis Model Mech. 2013;6(2):302-11. Epub 2013/01/29. doi: 10.1242/dmm.010934. PubMed PMID: 23355644; PubMed Central PMCID: PMCPMC3597013.
100. Schoenfeld G, Carta S, Rupprecht P, Ayaz A, Helmchen F. In vivo calcium imaging of CA3 pyramidal neuron populations in adult mouse hippocampus. eNeuro. 2021. Epub 2021/08/01. doi: 10.1523/ENEURO.0023-21.2021. PubMed PMID: 34330817.
101. Aharoni D, Hoogland TM. Circuit investigations with open-source miniaturized microscopes: past, present and future. Frontiers in cellular neuroscience. 2019;13:141.
102. Silva AJ. Miniaturized two-photon microscope: seeing clearer and deeper into the brain. Light: Science & Applications. 2017;6(8):e17104-e.
103. Lopes G, Bonacchi N, Frazao J, Neto JP, Atallah BV, Soares S, et al. Bonsai: an event-based framework for processing and controlling data streams. Front Neuroinform. 2015;9:7. Epub 2015/04/24. doi: 10.3389/fninf.2015.00007. PubMed PMID: 25904861; PubMed Central PMCID: PMCPMC4389726.
104. Thevenaz P, Ruttimann UE, Unser M. A pyramid approach to subpixel registration based on intensity. IEEE Trans Image Process. 1998;7(1):27-41. Epub 2008/02/13. doi: 10.1109/83.650848. PubMed PMID: 18267377.
105. Wirtshafter HS, Wilson MA. Locomotor and Hippocampal Processing Converge in the Lateral Septum. Current biology : CB. 2019;29(19):3177-92. doi: 10.1016/j.cub.2019.07.089. PubMed PMID: 31543450.
106. Olypher AV, Lansky P, Muller RU, Fenton AA. Quantifying location-specific information in the discharge of rat hippocampal place cells. J Neurosci Methods. 2003;127(2):123-35. Epub 2003/08/09. doi: 10.1016/s0165-0270(03)00123-7. PubMed PMID: 12906942.

Figure 1

A

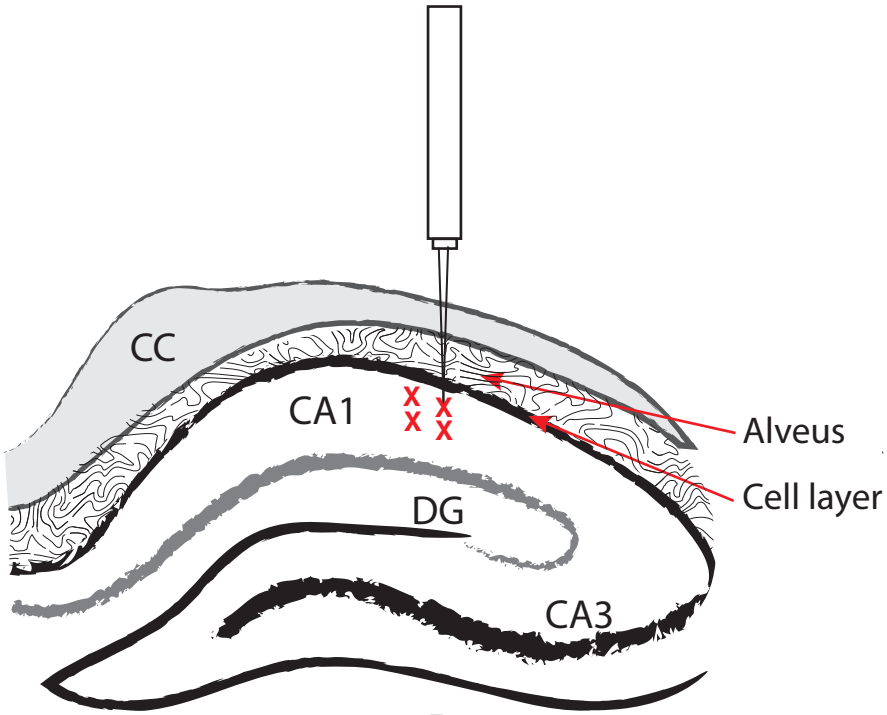
CC
CA1
DG
CA3
Alveus
Cell layer

B

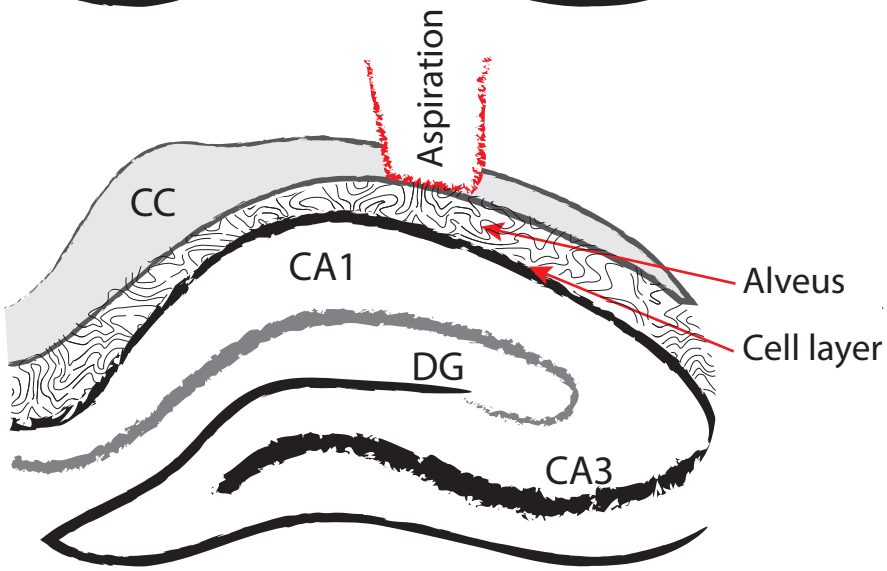
Aspiration
CC
CA1
DG
CA3
Alveus
Cell layer

C

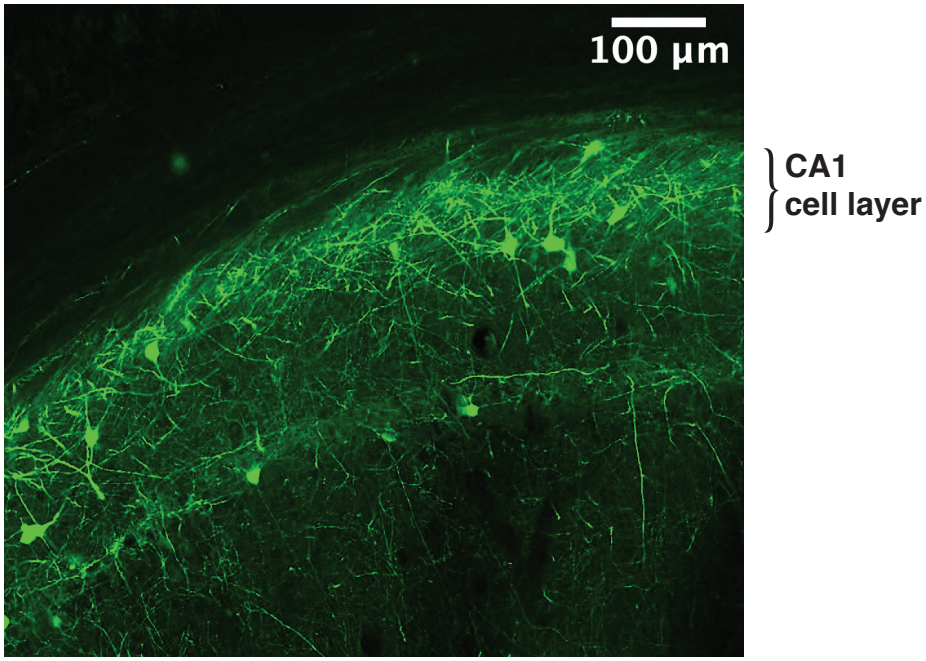
100 µm
CA1
cell layer

Figure 2

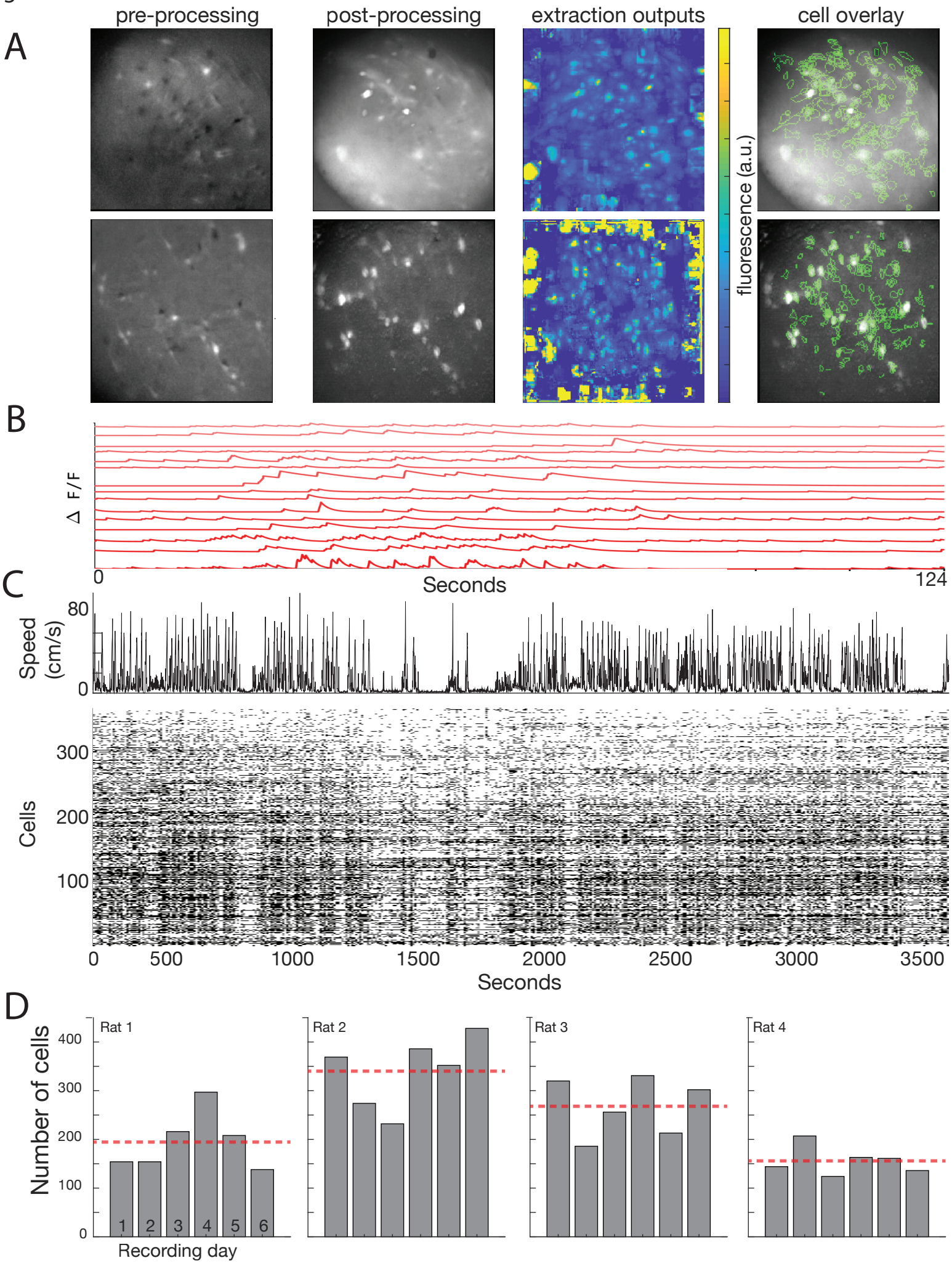
A
pre-processing
post-processing
extraction outputs
cell overlay
fluorescence (a.u.)
B
Δ F/F
0
Seconds
124
C
Speed (cm/s)
80
0
Cells
300
200
100
0
500
1000
1500
2000
2500
3000
3500
Seconds
D
Number of cells
400
300
200
100
0
Rat 1
Rat 2
Rat 3
Rat 4
1
2
3
4
5
6
Recording day

Figure 3

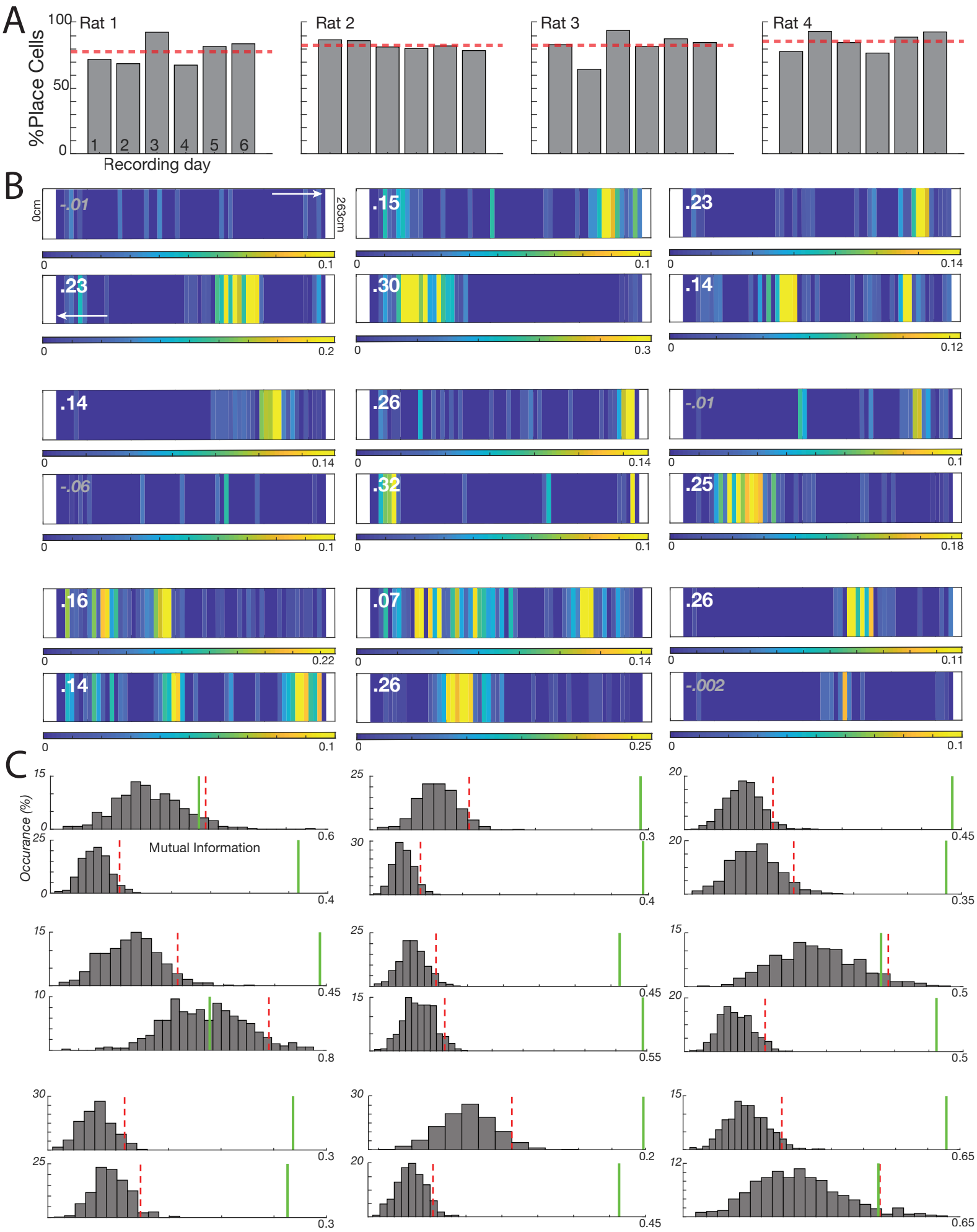
A
Rat 1
Rat 2
Rat 3
Rat 4
%Place Cells
100
50
0
1
2
3
4
5
6
Recording day
B
0cm
263cm
-.01
.15
.23
.23
.30
.14
.14
.26
-.01
-.06
.32
.25
.16
.07
.26
.14
.26
-.002
C
Occurance (%)
Mutual Information

Figure 4

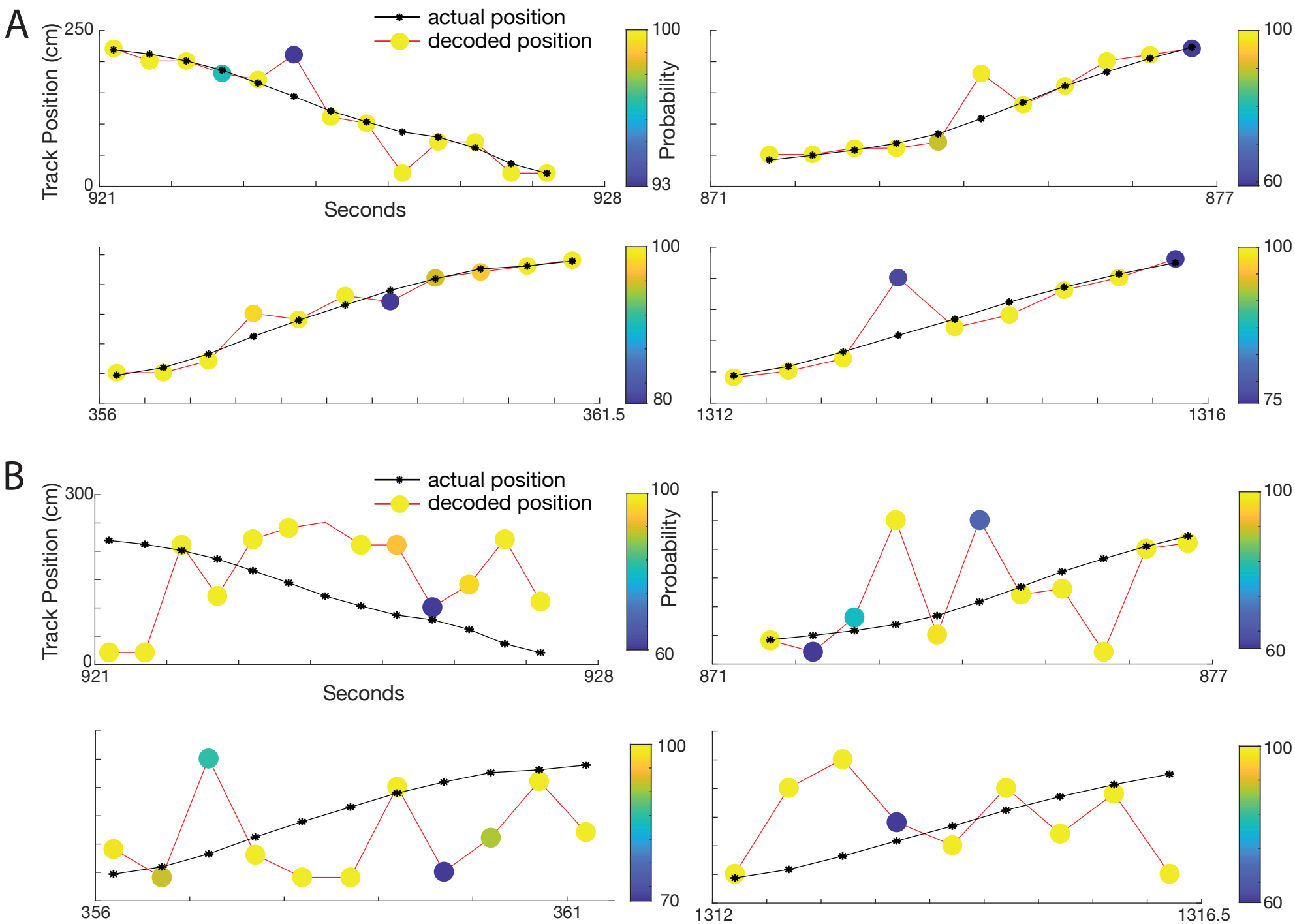
A
actual position
decoded position
Track Position (cm)
250
0
921
928
Seconds
Probability
100
93
871
877
100
60
356
361.5
100
80
1312
1316
100
75
B
actual position
decoded position
Track Position (cm)
300
0
921
928
Seconds
Probability
100
60
871
877
100
60
356
361
100
70
1312
1316.5
100
60

Figure 5

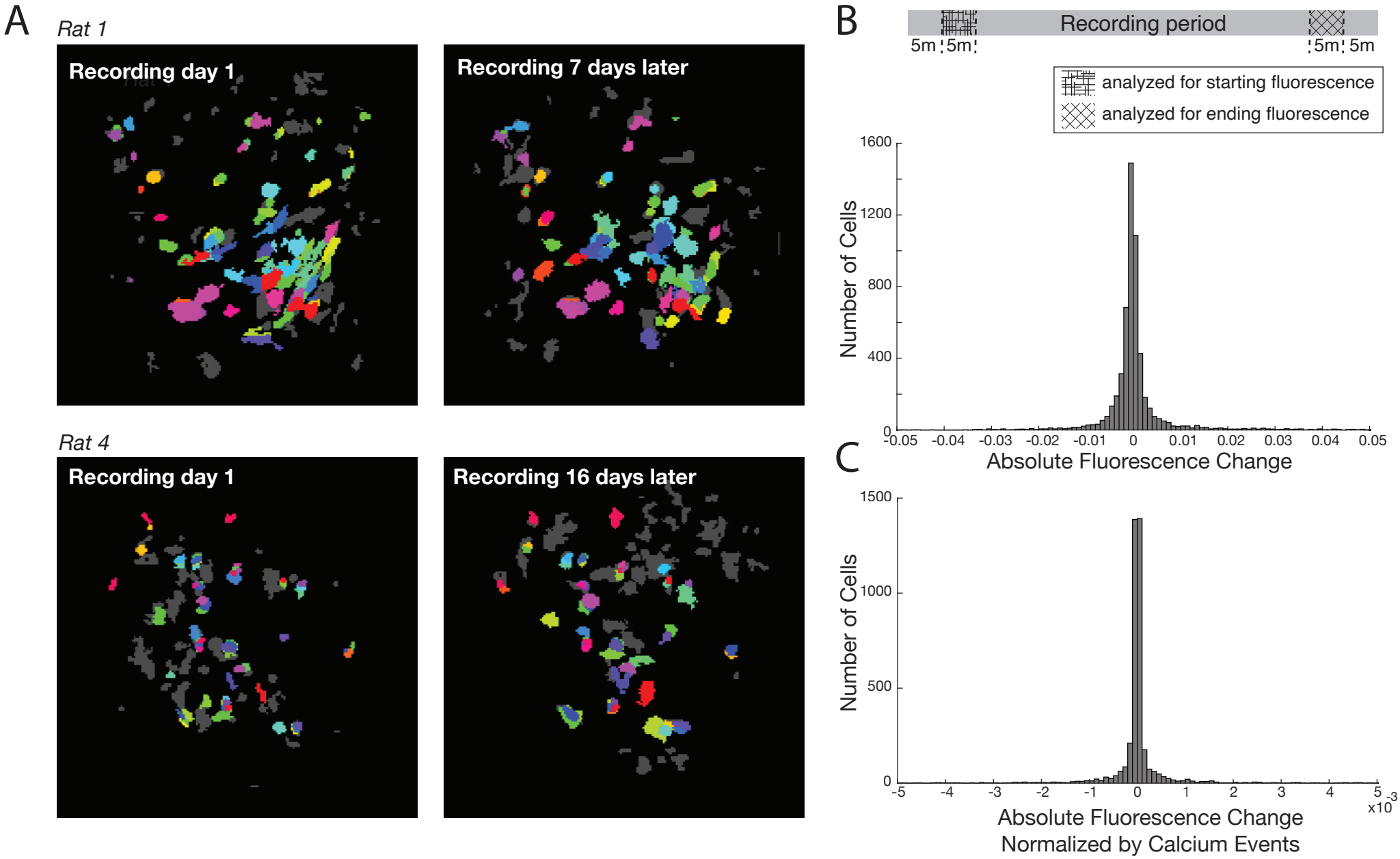
A
Rat 1
Recording day 1
Recording 7 days later
Rat 4
Recording day 1
Recording 16 days later
B
Recording period
5m
5m
5m
5m
analyzed for starting fluorescence
analyzed for ending fluorescence
Number of Cells
1600
1200
800
400
0
-0.05
-0.04
-0.03
-0.02
-0.01
0
0.01
0.02
0.03
0.04
0.05
Absolute Fluorescence Change
C
Number of Cells
1500
1000
500
0
-5
-4
-3
-2
-1
0
1
2
3
4
5
x10-3
Absolute Fluorescence Change
Normalized by Calcium Events

Figure S1

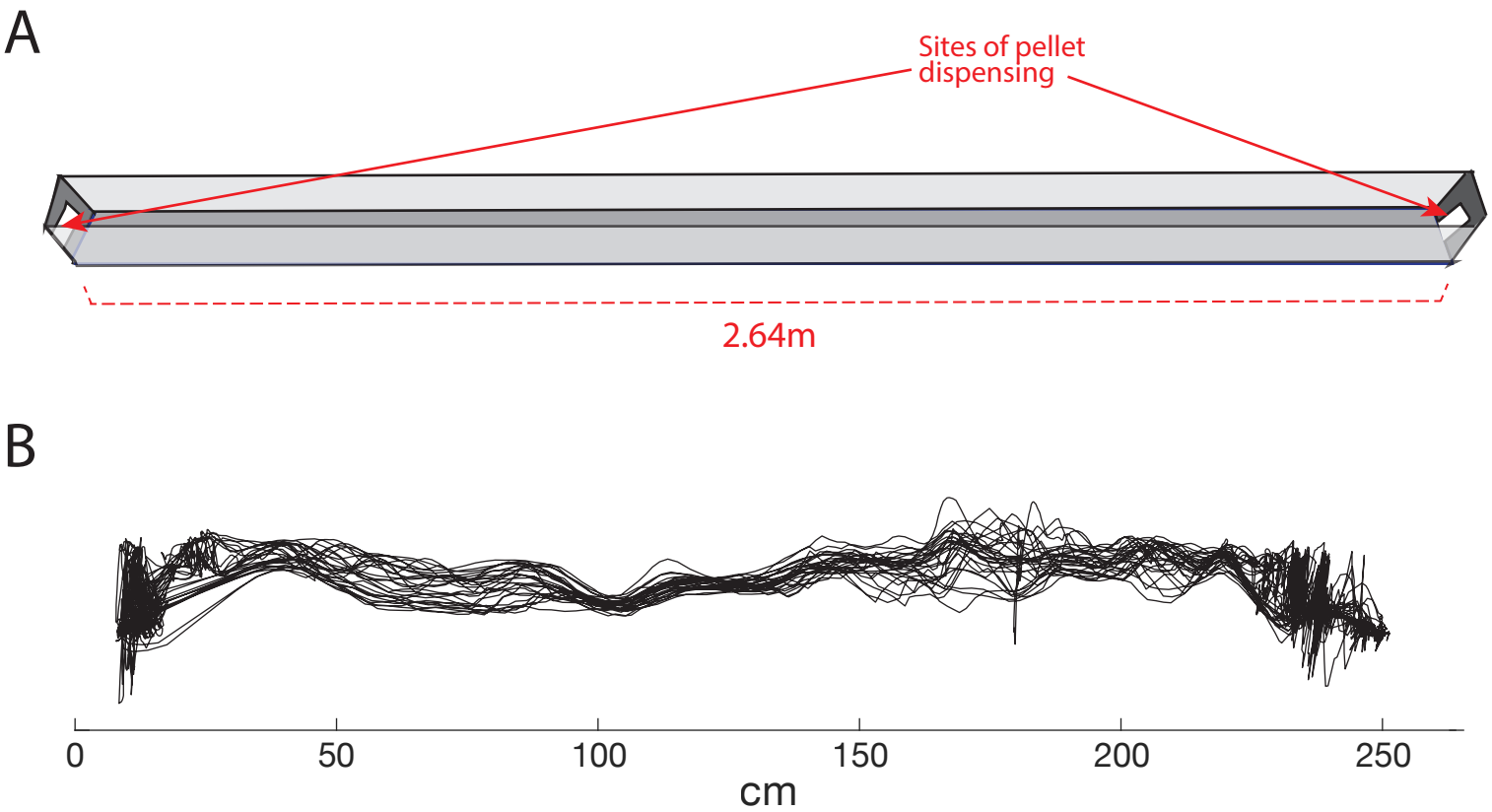

Figure S2

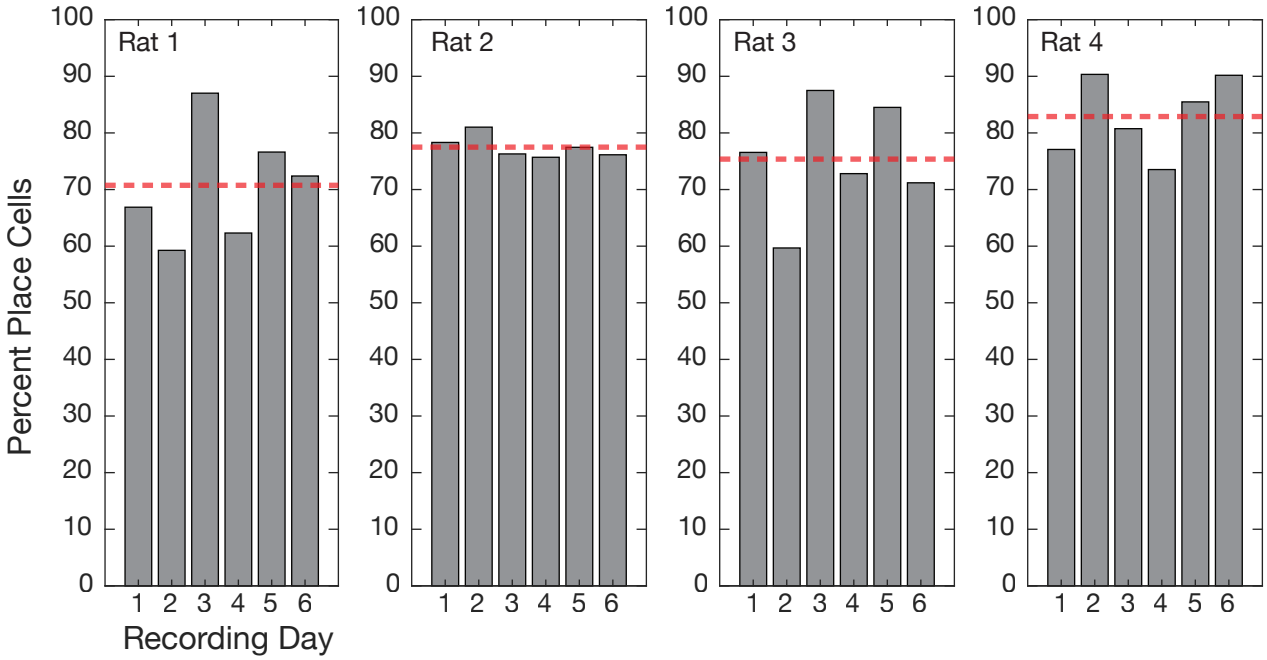
Rat 1
Rat 2
Rat 3
Rat 4
Percent Place Cells
Recording Day
0
10
20
30
40
50
60
70
80
90
100
1 2 3 4 5 6